ISCI, Volume *3*

Supplemental Information

Alternating-Magnetic-Field-Mediated Wireless Manipulations of a Liquid Metal for Therapeutic Bioengineering

Yue Yu and Eijiro Miyako

Supplemental Figures

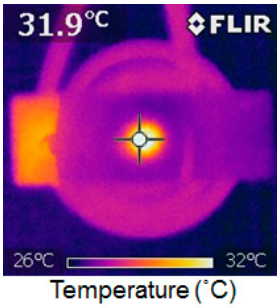

Fig. S1. Related to Fig. 1. Infrared image of LM (40 μL) heated by momentary ON–OFF switching of the AMF (250 A m^{-1}, 245 kHz).

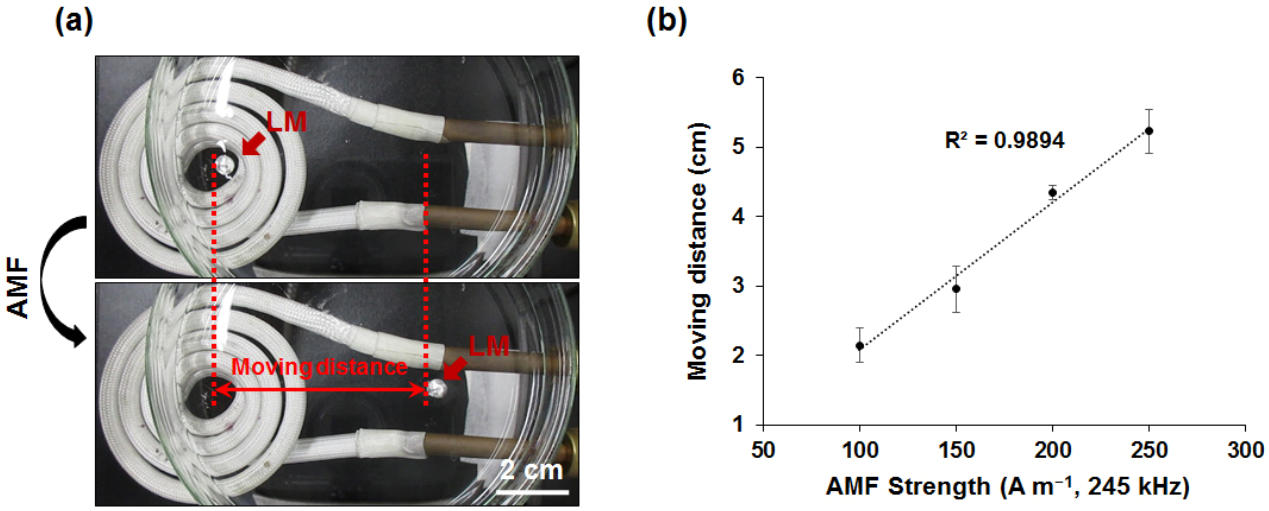

Fig. S2. Related to Fig. 2. Depiction (a) and statistics results (b) of LM moving distance by ON–OFF switching AMF. Data are represented as mean ± SEM.

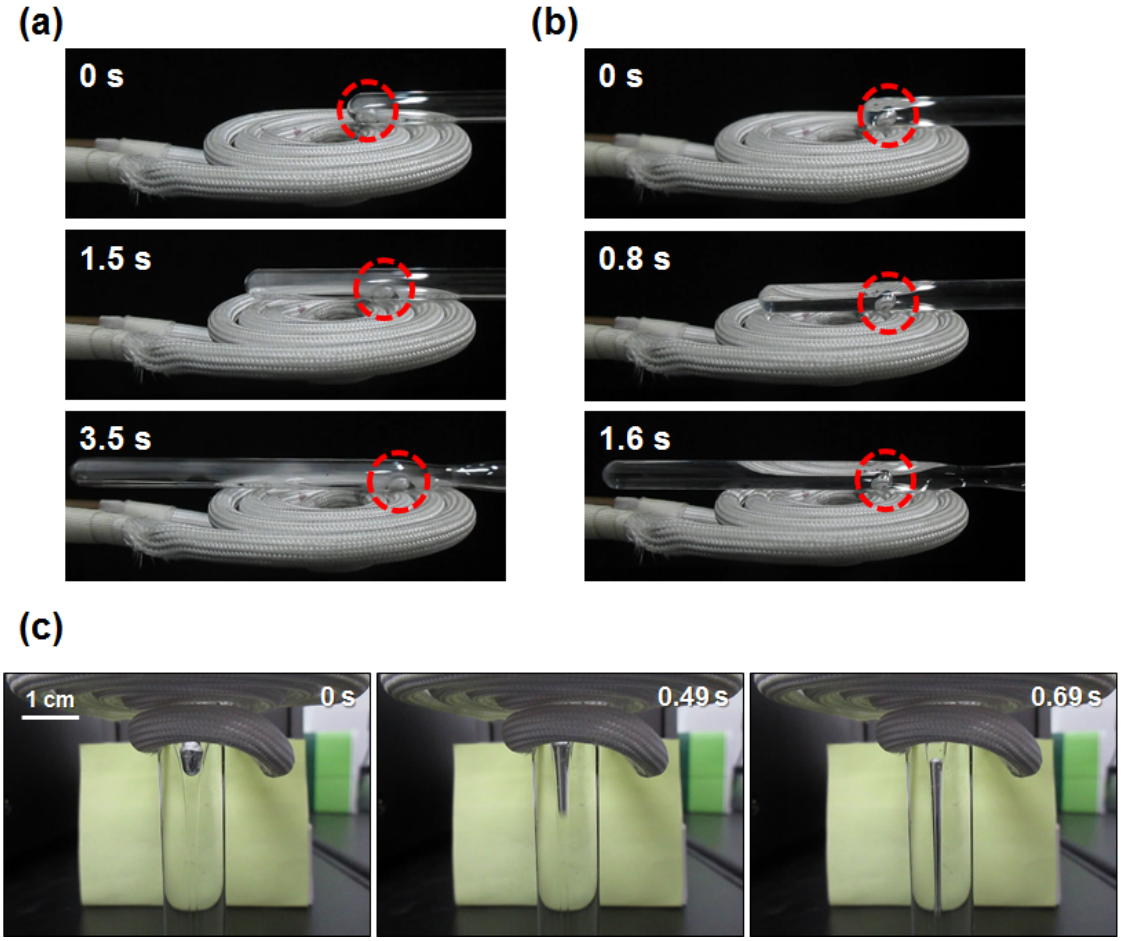

Fig. S3. Related to Fig. 2. Sequential snapshots of AMF-induced (100 A m^{-1}, 245 kHz) relative movement (to the glass tube) of LM blob (30 µL) (a) without or (b) with water. (c) Time-lapsed images revealing the flexible LM (30 µL) movement in a Pasteur pipette with water via AMF-induction (90 A m^{-1}, 245 kHz).

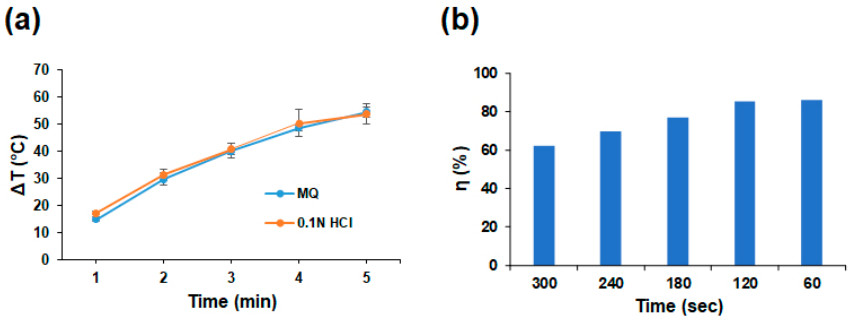

Fig. S4. Related to Fig. 3 and Experimental Procedures. (a) Temperature increasing curves of LM (30 µL) with or without oxidized layer in 5 mL media under AMF application (200 A m^{-1}, 245 kHz). Data are represented as mean ± SEM. (b) AMF−thermal conversion efficiency (η) of LM (30 µL) in MQ water (5 mL) after AMF application (200 A m^{-1}, 245 kHz) over a period of time (60, 120,180, 240 and 300 sec, respectivery).

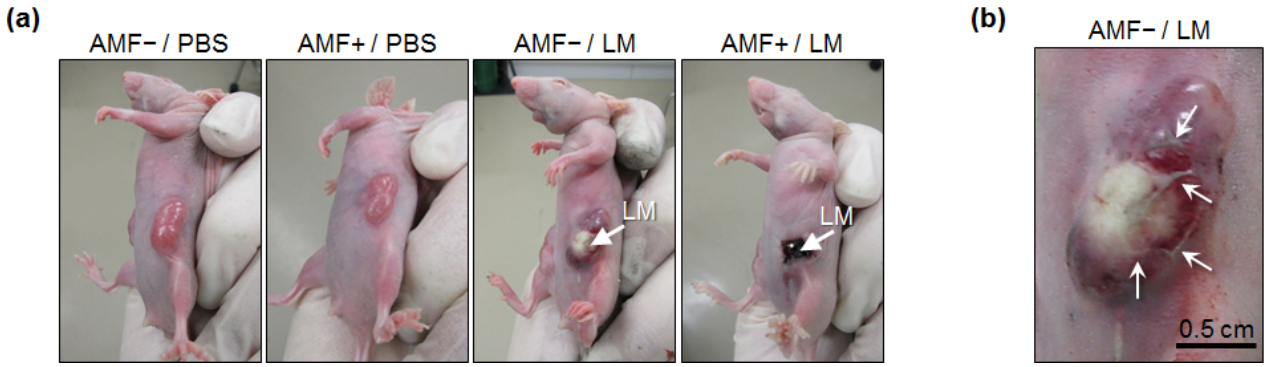

Fig. S5. Related to Fig. 5. (a) Representative images of a tumor injected with 30 μL of LM or PBS at 24 h post AMF treatment (150 A m^{-1}, 245 kHz). White arrows indicate the LM injection sites. (b) Representative image of tumor blood capillaries obstructed by the LM (white arrows).

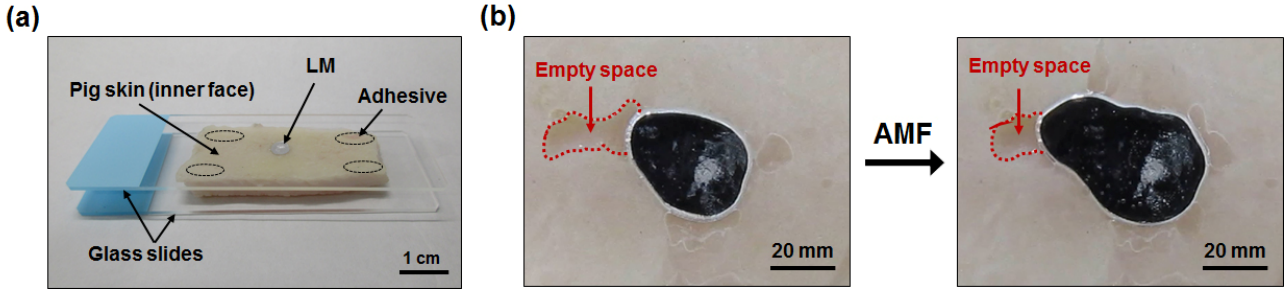

Fig. S6. Related to Figs. 4 and 5. AMF-induced LM transformation in *ex vivo* model. (a) Depiction of sandwich fabrication for simulation of AMF-induced LM subcutaneously transformation. (b) Transformation behavior of LM (30 μL) deposited between a glass slide and a piece of pig skin under AMF application (100 A m^{-1}, 245 kHz).

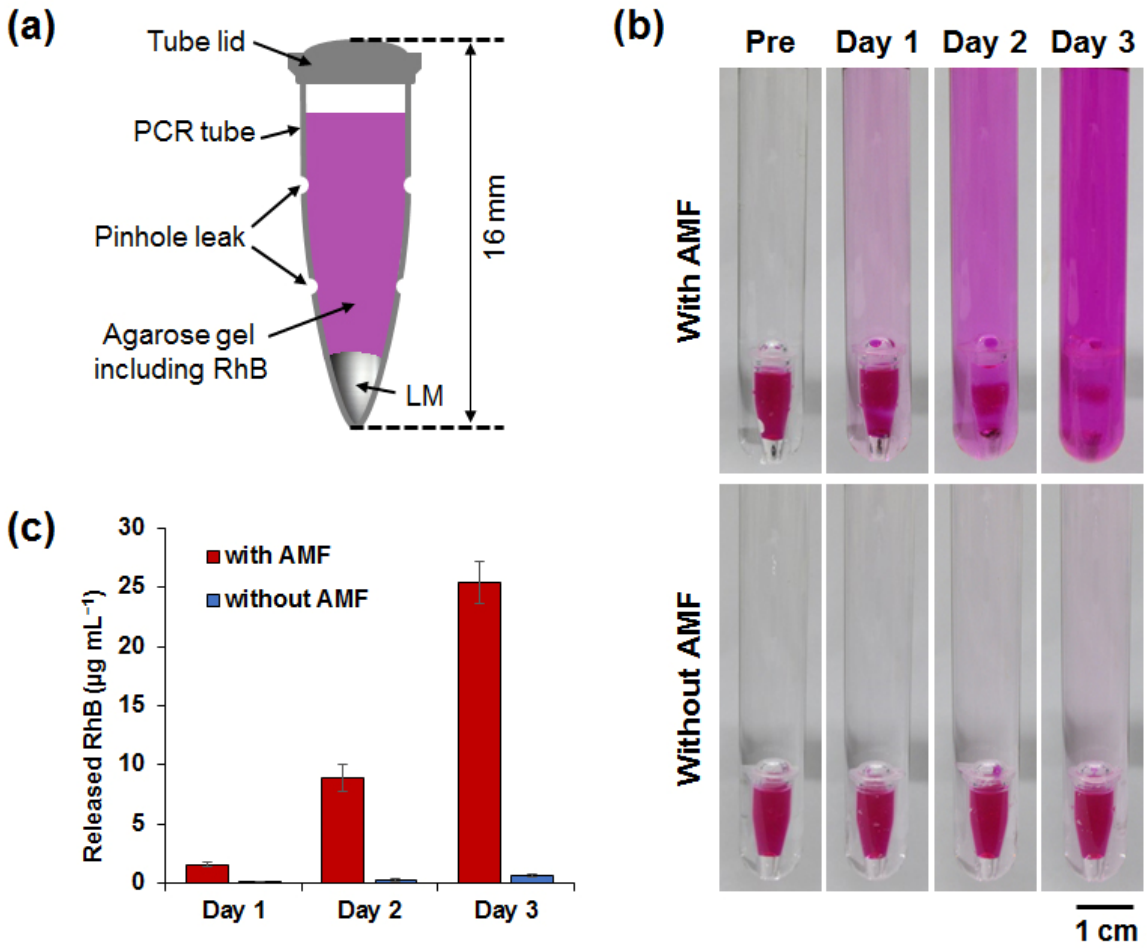

Fig. S7. Related to Fig. 6. (a) Depiction of LM/RhB-Gel capsule designed for long-termed drug (RhB) release. The capsule is composed of LM (30 μL), agarose (2%, w/w, 300 μL), RhB (1 mg mL^{-1}) and a PCR tube with four pinholes (diameter: 500 μm) on the wall. (b) Photographs and (c) quantitation of RhB release behavior from the capsule by AMF induction over 3 days. AMF (200 A m^{-1}, 245 kHz) was applied for 1 min once per day. Data are represented as mean ± SEM. The released RhB amount in water was determined by UV-vis absorption immediately after AMF induction. The system was kept at 37°C except when AMF was applied.

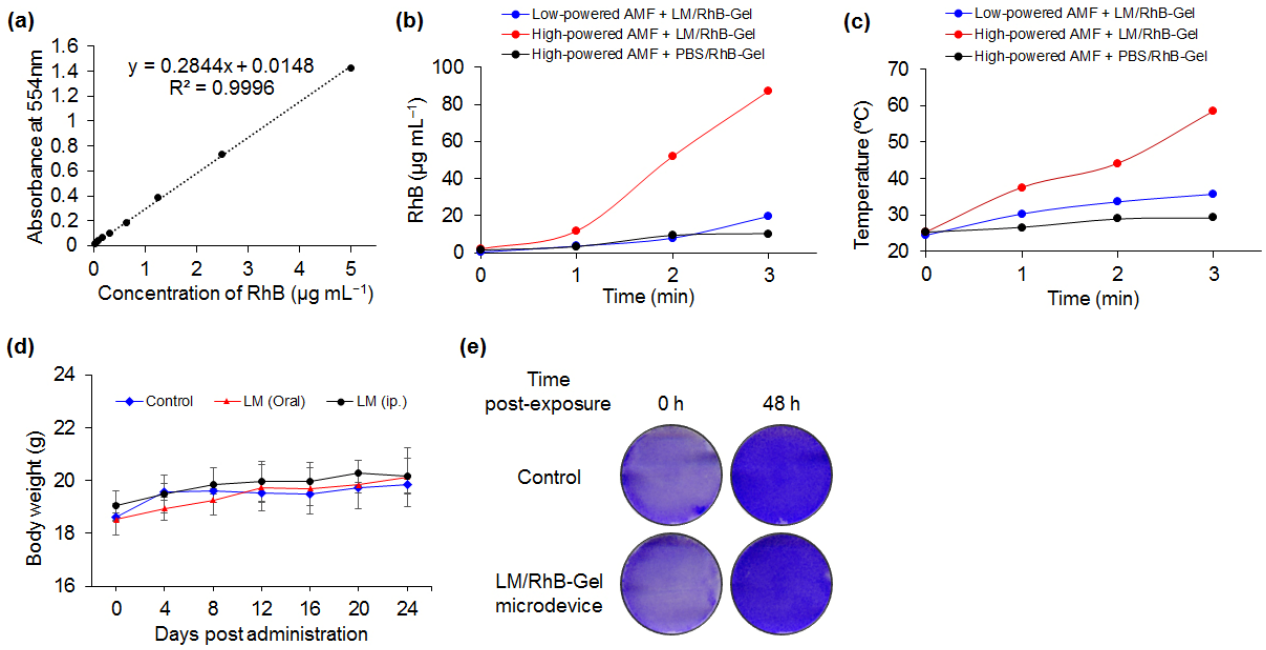

Fig. S8. Related to Fig. 6. (a) UV–vis calibration of RhB in water. (b) Release profile of RhB into 5 mL of water from the LM/RhB-Gel microdevice (LM 20 μL; 2% w w^{-1} agarose 200 μL; RhB, 0.5 mg mL^{-1}) under exposure to a low- (100 A m^{-1}, 245 kHz) or high-powered (100 A m^{-1}, 245 kHz) AMF over a period of time. The PBS/RhB-Gel microdevice in which the LM was replaced with the same amount of PBS served as the control. (c) Temperature increase of the LM/RhB-Gel microdevice immersed in 5 mL of water over period of time under exposure to a low- (100 A m^{-1}, 245 kHz) or high-powered (100 A m^{-1}, 245 kHz) AMF. The PBS/RhB-Gel microdevice with the LM replaced with the same amount of PBS served as the control. (d) Body weight of mice with different administrations of LM. Data are represented as mean ± SEM. (e) Crystal violet staining of TIG-3 with or without the LM/RhB-Gel microdevice under low-powered AMF exposure. Microdevices were incubated with cells in 3 mL of culture medium and were heated by an AMF (100 A m^{-1}, 245 kHz) for 2 min. Staining was performed immediately after treatment and 48 h later.

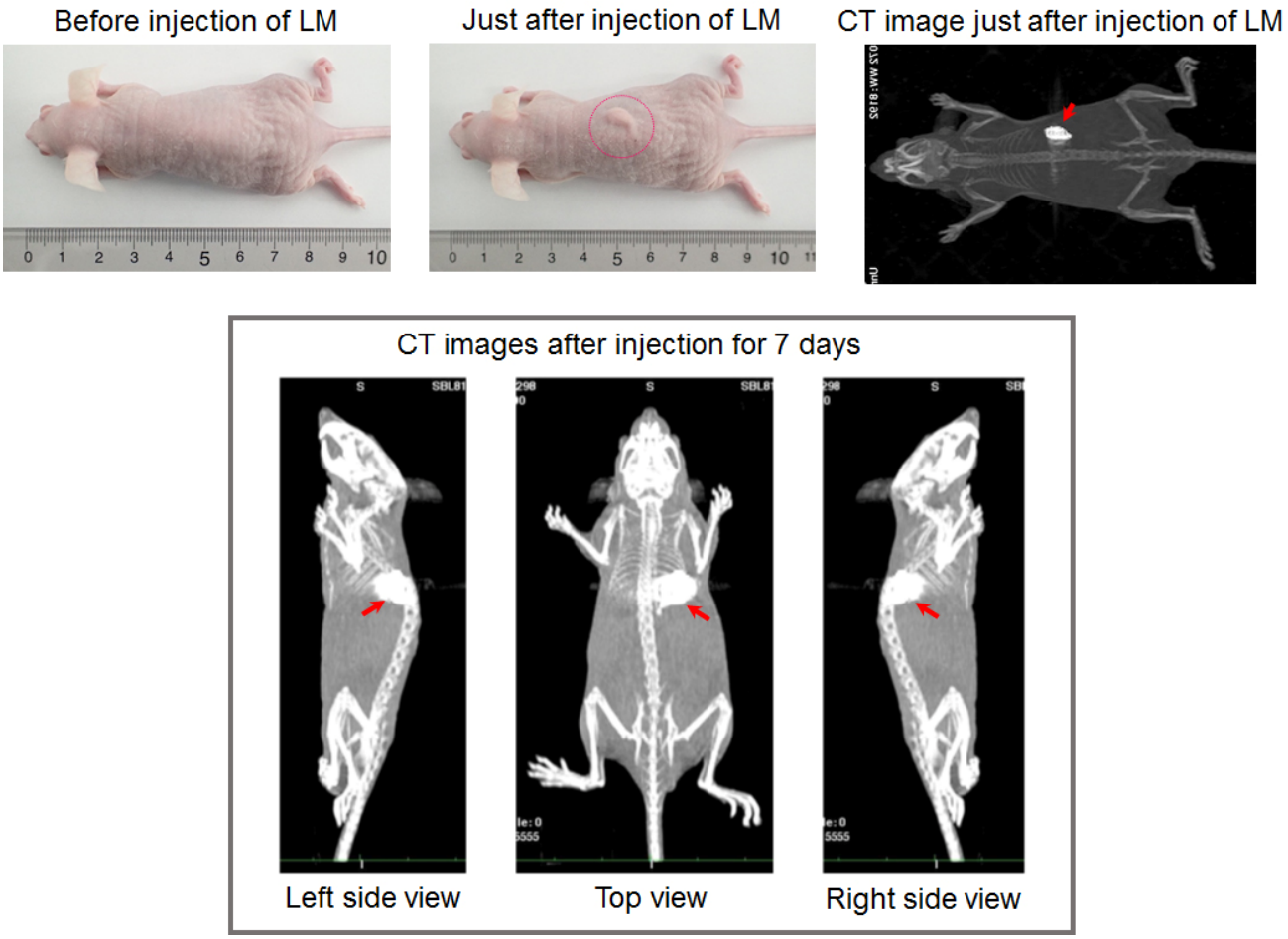

Fig. S9. Related to Fig. 6. Three-dimensional-X-ray images of LM (30 μL)-injected living mice (n = 4) immediately after subcutaneous administration and after injection for 7 days. Red circles indicate LM-injected site. Red arrows display the LM.

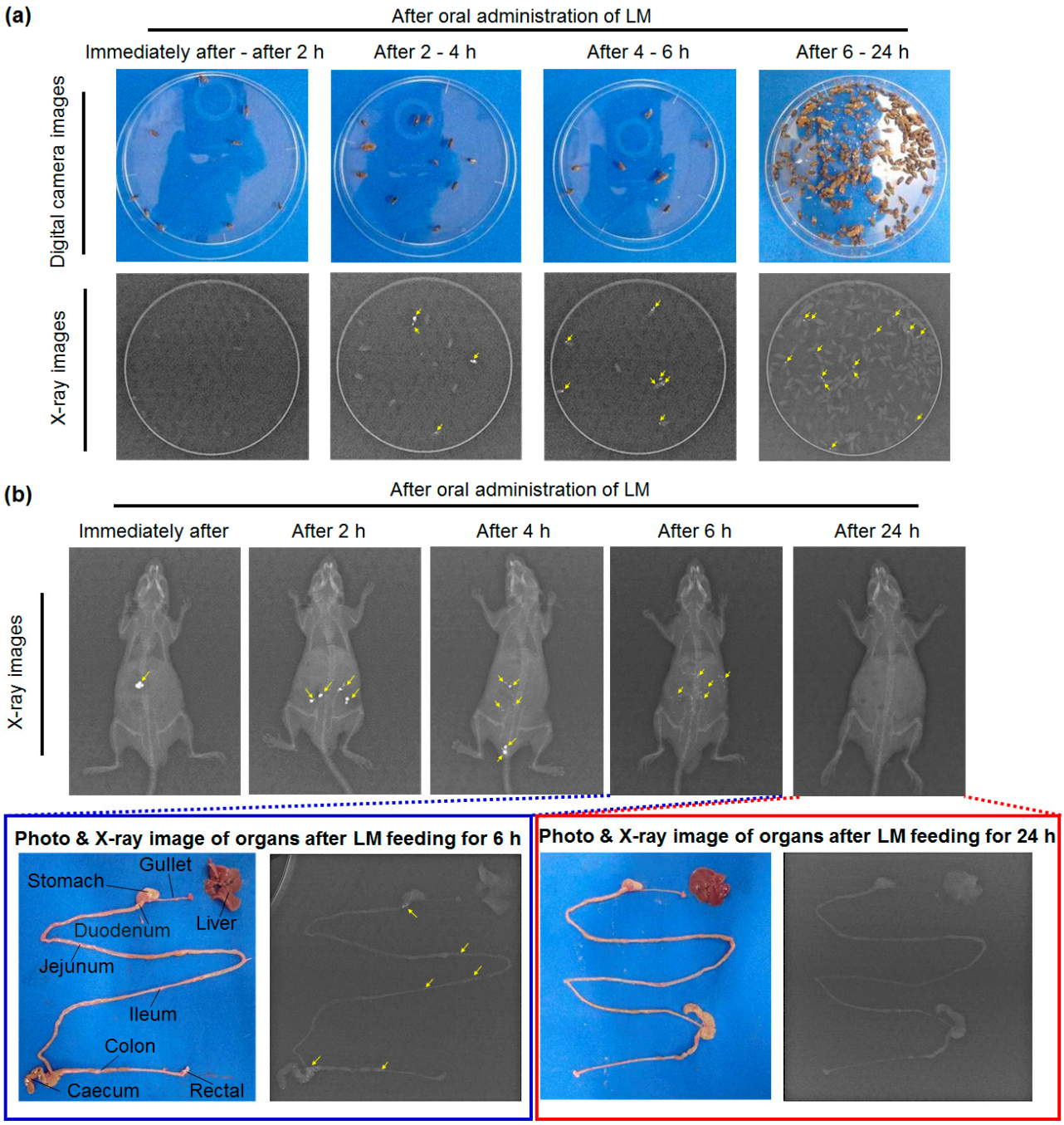

Fig. S10. Related to Fig. 6. X-ray images of LM (5 μL)-fed living mice (n = 3) after oral administration. (a) Photos and X-ray images of feces after oral feeding of LM for 24 h. (b) Photos and X-ray images of mice and organs after oral feeding of LM for 24 h.

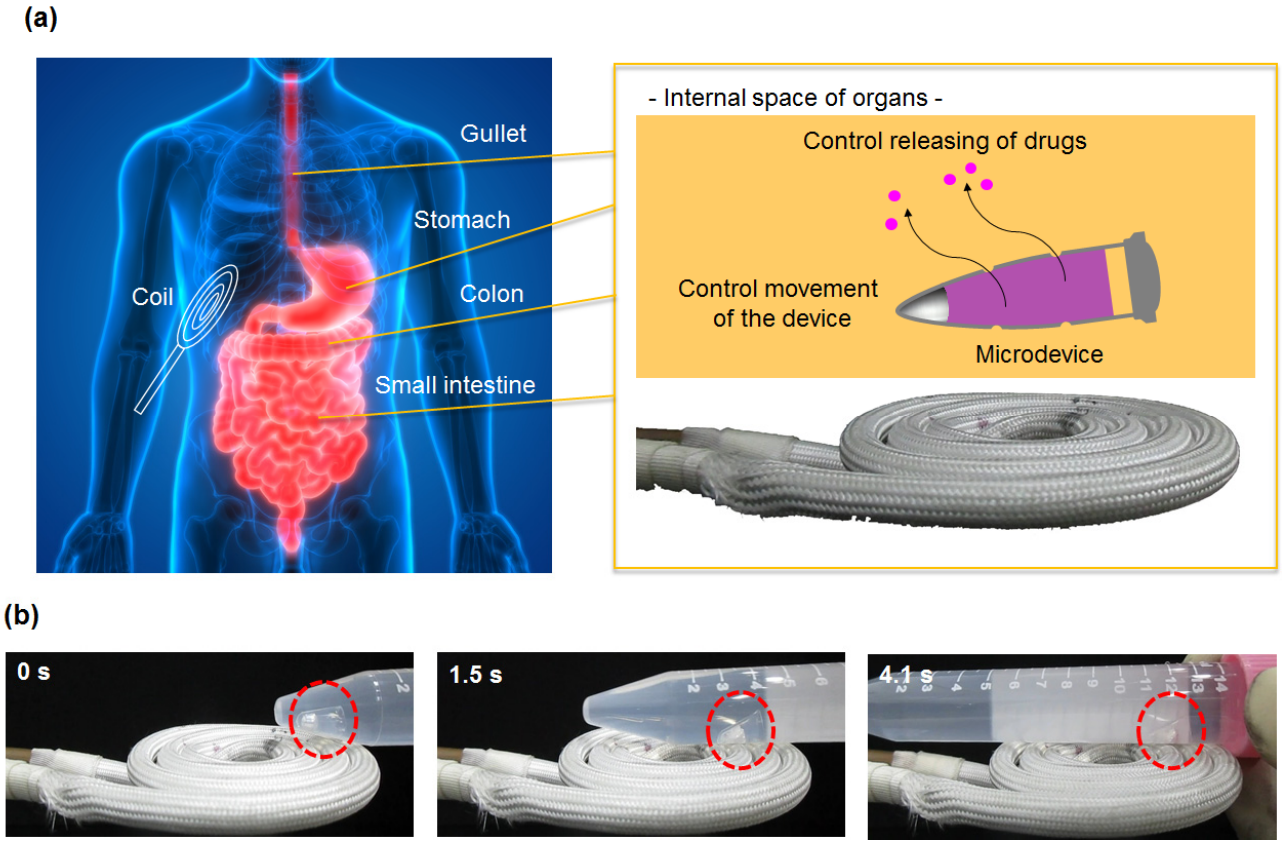

Fig. S11. Related to Fig. 6. (a) Schematic illustrations of utilities of LM/Gel microdevice in digestive organs for advanced drug delivery system, respectively. (b) Sequential snapshots of AMF-induced (100 A m^{-1}, 245 kHz) relative movement (to the falcon tube) of LM/Gel microdevice (LM 30 μL; 2% w/w agarose 200 μL) in PBS.

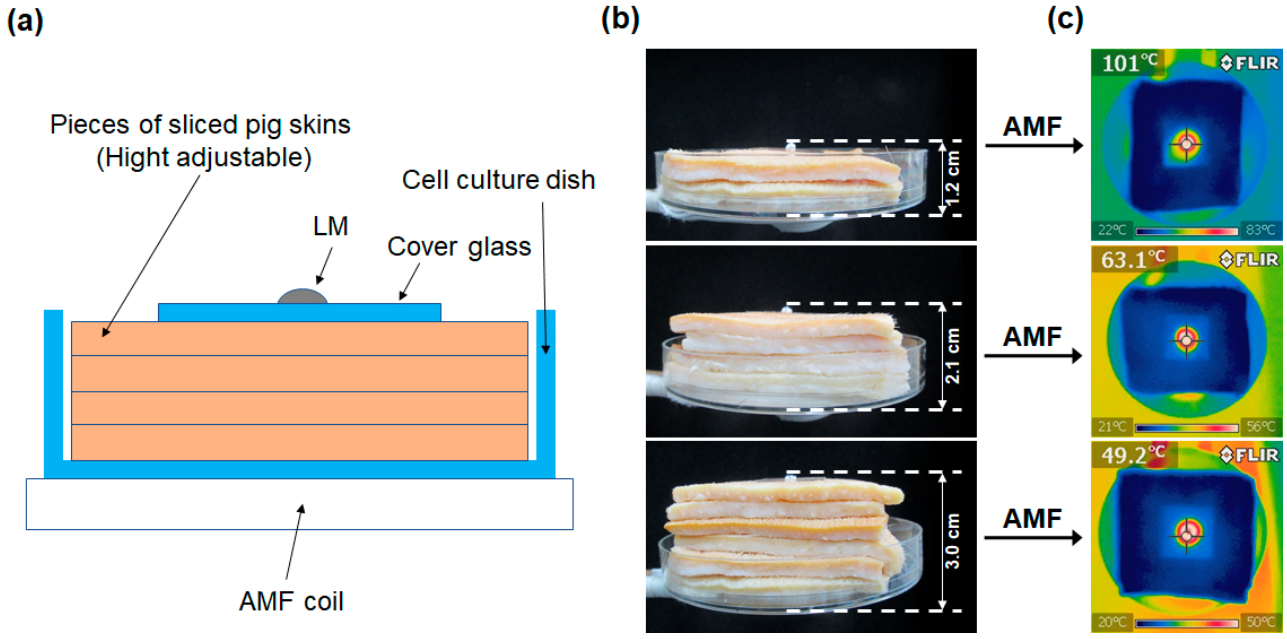

Fig. S12. Related to Fig. 6. Effect of AMF on depth penetration through biological tissues for LM heating. (a) Schematic illustration of the experimental set up. (b) LM (30 μL) was deposited on pig skins with different heights to AMF coil. (c) The thermal images of LM after AMF application (270 A m^{-1}, 245 kHz) for 10 seconds.

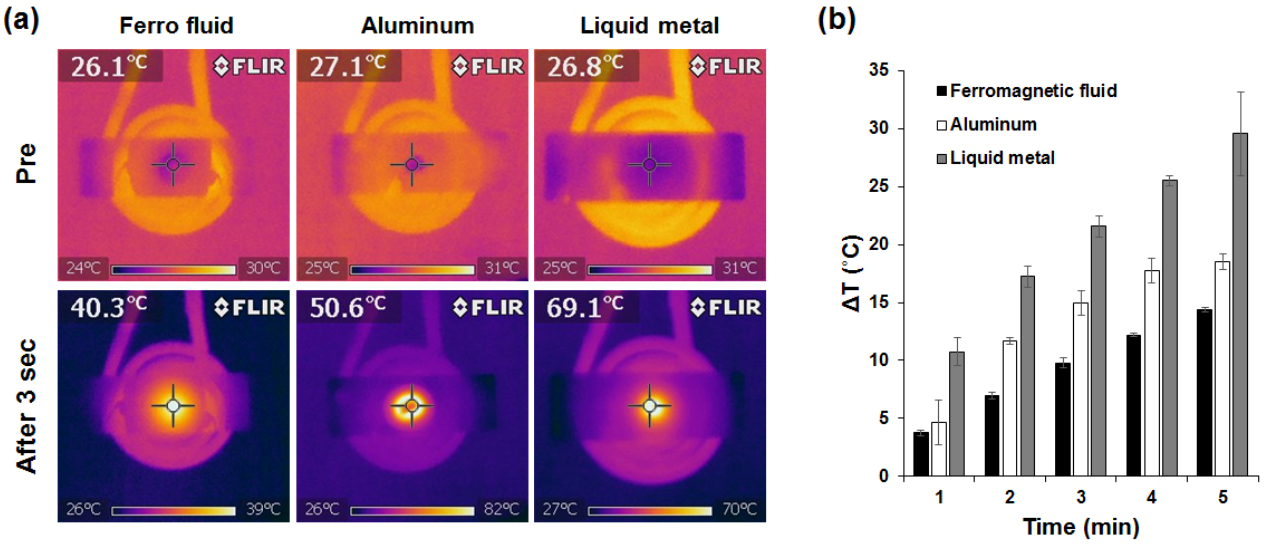

Fig. S13. Related to Figs. 3 and 6. (a) Thermal images of 100 mg of ferromagnetic fluid, aluminum and LM in air before and after AMF application (150 A m^{-1}, 245 kHz) for 3 sec. (b) Heating behavior comparison of various materials (100 mg) immersed in water (10 mL) over period of time under AMF exposure (200 A m^{-1}, 245 kHz). Data are represented as mean ± SEM.

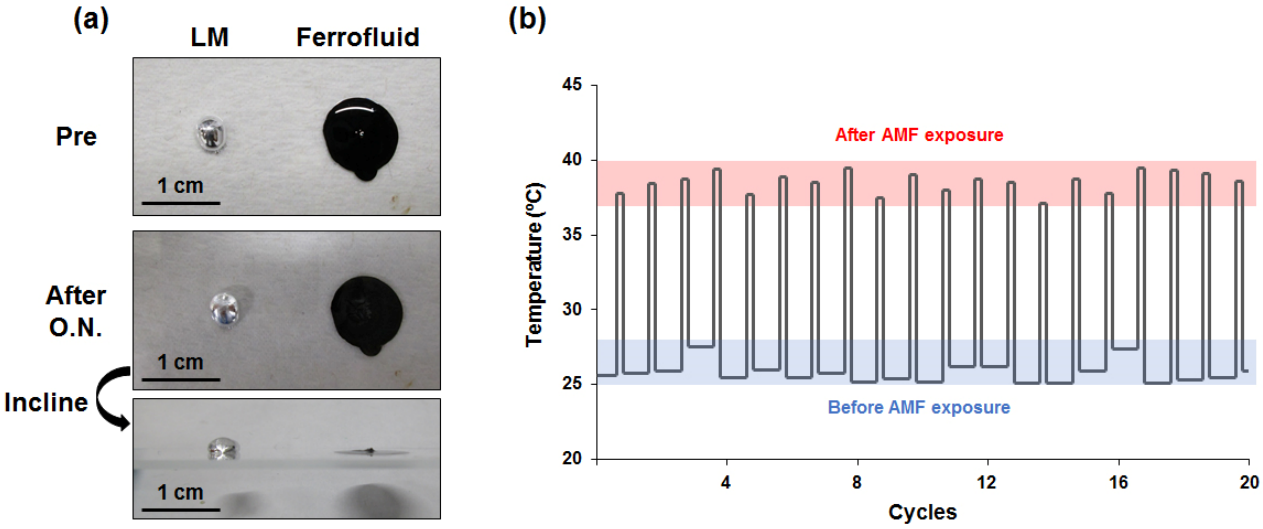

Fig. S14. Related to Figs.3 and 6. (a) Air-stable performance of LM and ferromagnetic fluid. Photographs showing 30 μL of LM and ferromagnetic fluid before and after being exposed to ambient air at room temperature for overnight. (b) LM thermal stability over 20 heating/cooling cycles. LM (50 μL) was immersed in PBS (10 mL) and exposed to AMF (200 A m^{-1}, 245 kHz) for 1 min. Temperatures before and after AMF exposure were recorded as one cycle.

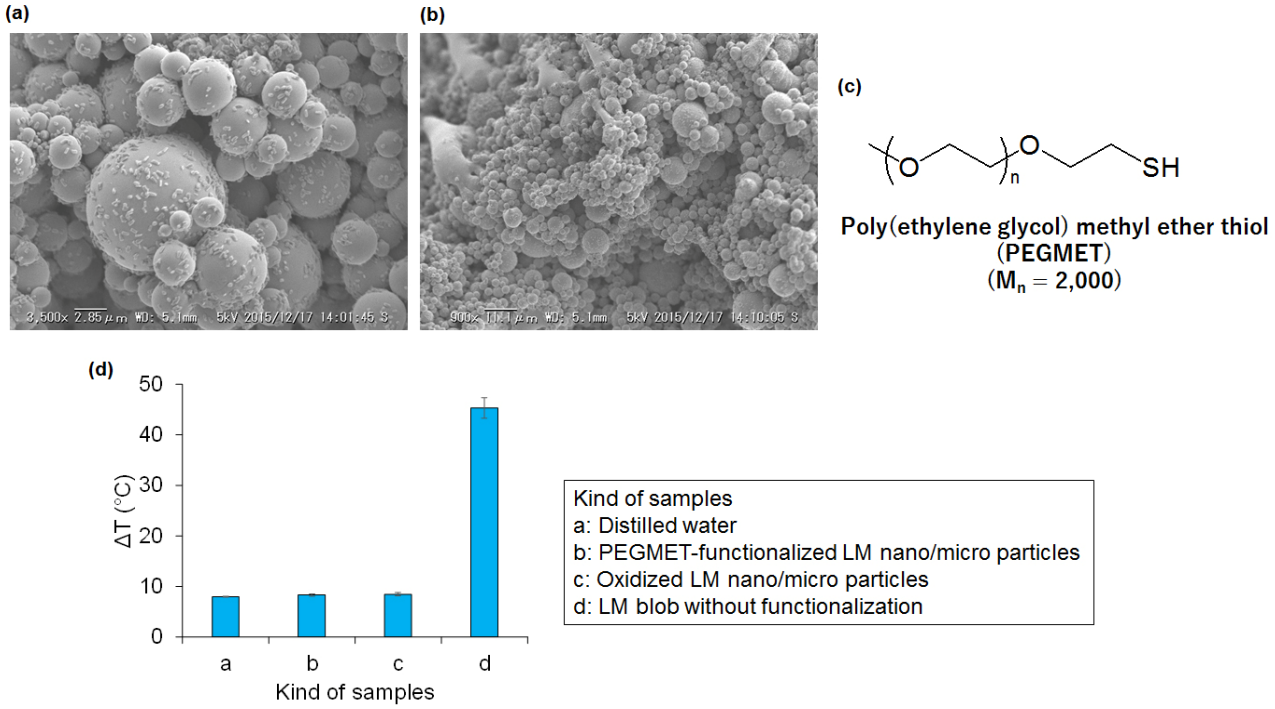

Fig. S15. Related to Figs. 3 and 6. SEM images of (a) oxidized LM nano/micro particles and (b) PEGMET-functionalized LM nano/microparticles. (c) Chemical structure of PEGMET. (d) AMF (270 A m^{-1}, 245 kHz)-induced temperature increasing behabiours of variusou LM samples in distilled water (5mL). LM concetration: 100 mg, AMF duration: 3 min. Data are represented as mean ± SEM.

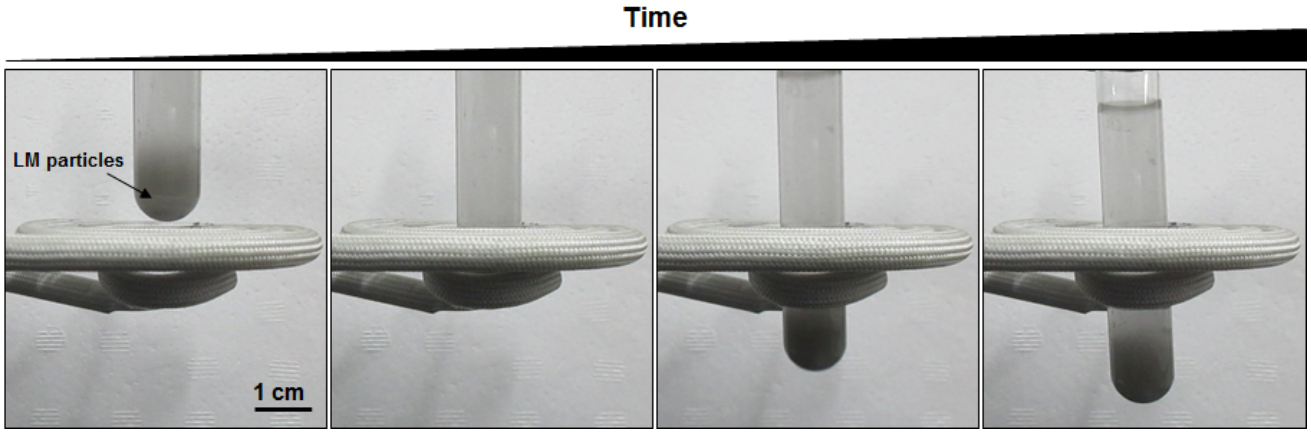

Fig. S16. Related to Figs. 1, 2 and 6. Sequeantial snapshots of LM nano/micro particles under AMF. LM: 100 mg in 5mL water, AMF: 250 A m^{-1}, 245 kHz.

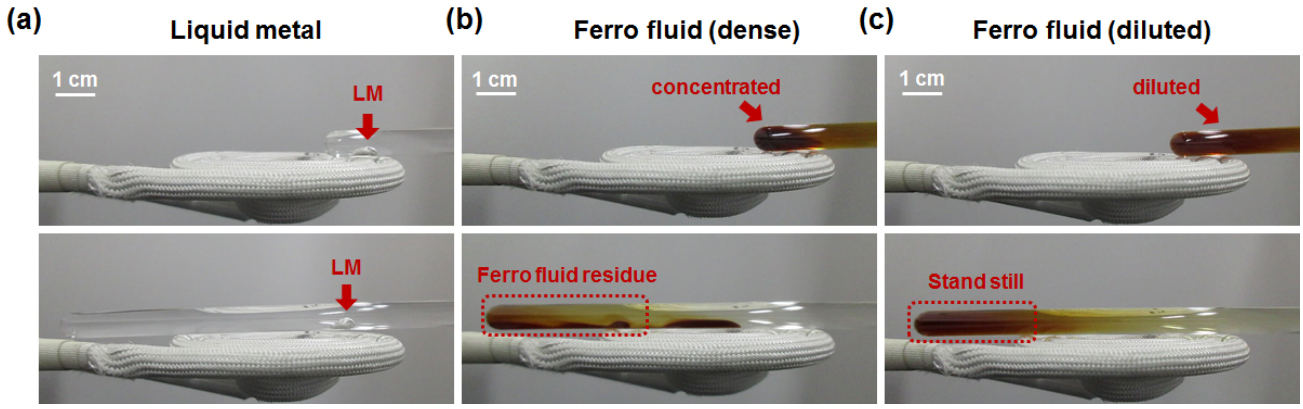

Fig. S17. Related to Figs. 1, 2 and 6. Sequential snapshots of AMF-induced (150 A m^{-1}, 245 kHz) relative movement (comparing to glass tube) of (a) LM blob, (b) dense and (c) diluted ferro fluids in the aqueous solution.

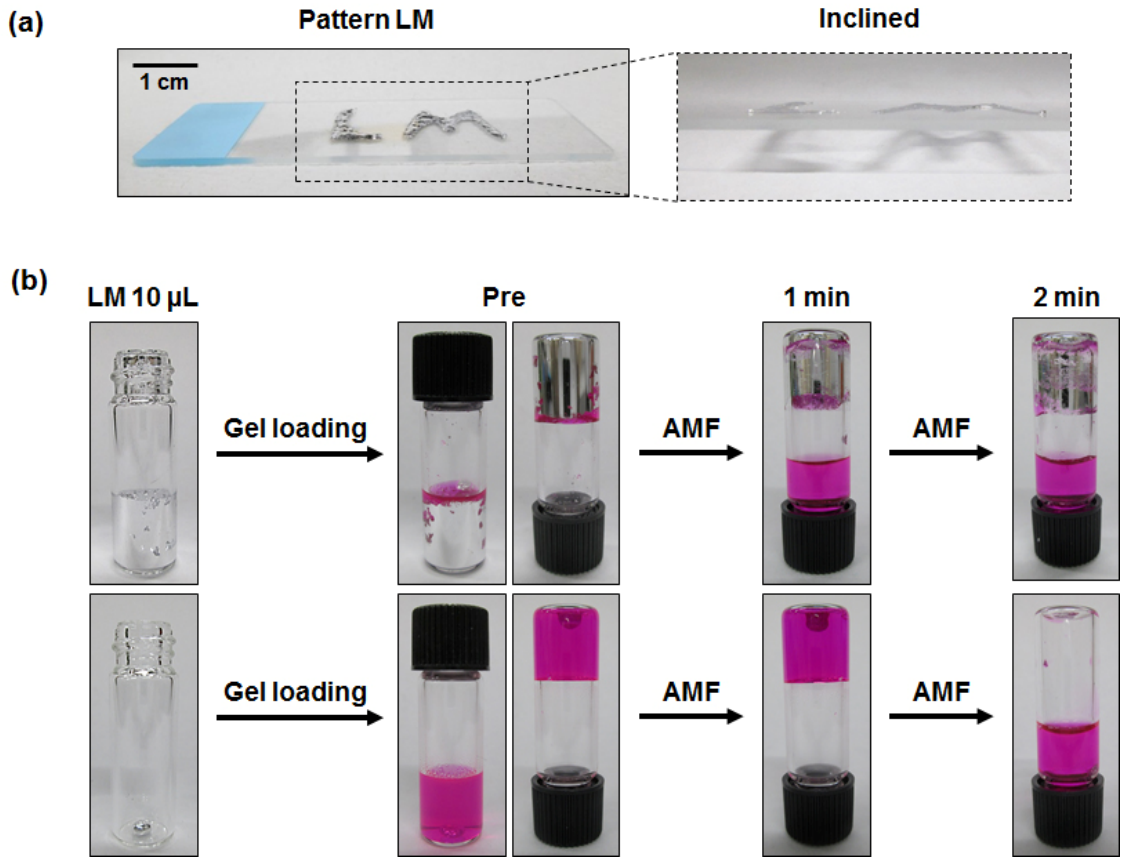

Fig. S18. Related to Fig. 6. (a) Patterning LM layer (50 μL totally) on a glass slide. (b) Drug releasing behabiours in comparison with LM in different forms (spherical droplet and spreading layer) under AMF. LM: 10 μL, hydrogel matrix: 500 μL (agarose: 2% w w^{-1}; RhB, 0.1 mg mL^{-1}), AMF: 150 A m^{-1}, 245 kHz.

Table S1 Related to Fig. 6. Complete blood cell count (CBC) and biochemical examination after 28 days*.

Methods	Entry**	Unit	Subcutaneous injection (n = 5)		
			LM	PBS	p value
CBC	WBC	$\times 10^2\ \mu L^{-1}$	71.8 ± 5.3	75.4 ± 15.4	> 0.05
	RBC	$\times 10^4\ \mu L^{-1}$	901.4 ± 37.6	894.2 ± 13.3	> 0.05
	HGB	$g\ dL^{-1}$	14.1 ± 0.6	14.2 ± 0.3	> 0.05
	HCT	%	41.5 ± 1.9	41.3 ± 0.5	> 0.05
	MCV	fL	46.0 ± 0.4	46.2 ± 0.3	> 0.05
	MCH	pg	15.7 ± 0.1	15.8 ± 0.3	> 0.05
	MCHC	$g\ dL^{-1}$	34.0 ± 0.4	34.3 ± 0.4	> 0.05
	PLT	$\times 10^4\ \mu L^{-1}$	70.4 ± 4.2	70.8 ± 5.9	> 0.05
Biochemical exam	CRP	$\mu g\ mL^{-1}$	1.3 ± 0.1	1.6 ± 0.5	> 0.05
	AST	$IU\ L^{-1}$	59.8 ± 10.7	77.8± 31.9	> 0.05
	ALT	$IU\ L^{-1}$	33.0 ± 5.2	36.2 ± 14.2	> 0.05
	LDH	$IU\ L^{-1}$	246.0 ± 77.3	325.8 ± 138.3	> 0.05
	AMY	$IU\ L^{-1}$	1723.4 ± 156.0	1654.0 ± 179.1	> 0.05
	CK	$IU\ L^{-1}$	164.0 ± 54.4	231.0 ± 179.0	> 0.05
	TP	$g\ dL^{-1}$	4.1 ± 0.1	4.0 ± 0.1	> 0.05
	ALB	$g\ dL^{-1}$	2.8 ± 0.1	2.7 ± 0.2	> 0.05
	CRE	$mg\ dL^{-1}$	0.1 ± 0.01	0.1 ± 0.02	> 0.05

*The date shows average values from five experiments. Values in brackets indicate standard deviation.

**Abbreviations: WBC (white blood cell), RBC (red blood cell), HGB (hemoglobin), HCT (hematocrit), MCV (mean corpuscular volume), MCH (mean corpuscular hemoglobin), MCHC (mean corpuscular hemoglobin concentration), PLT (platelet), CRP (C-reactive protein), AST (aspartate aminotransferase), ALT (alanine aminotransferase), LDH (lactate dehydrogenase), AMY (amylase), CK (creatine kinase), TP (total protein), ALB (albumin), CRE (creatinine). Results were presented in the form of mean ± standard deviation, with “n” indicating the number of samples per group. Statistical analyses were performed using Student’s t-tes

Transparent Methods

AMF-induced temperature increase

All heat-dissipation experiments were performed using an EasyHeat device (Ambrell, NY, USA) consisting of a transistor inverter and a sample coil enclosure powered by an AC power supply. AMF-induced temperature increases were investigated as follows. A droplet of LM (Ga:In = 75.5:24.5 wt%; Alfa Aesar, Ward Hill, MA, USA) (25 μL, ~100 mg) was immersed into distilled water (5 mL) followed by AMF exposure under various conditions as indicated. The temperature of the solutions was measured in real time using a temperature sensor (AD-5601A; A&D, Tokyo, Japan). The LM droplet surface temperature after AMF heating was monitored by infrared (IR) thermography (i7; FLIR, Nashua, NH, USA).

For the heating stability and comparison experiments, the same methods mentioned above was performed with ferrofluid [sodium tetradecene sulfonate-functionalized magnetite (Fe_3O_4) nanoparticles, concentration of Fe_3O_4 is 35 wt%, diameter of nanoparticles is about 10 nm, and solvent is distilled water] (M-300, Sigma Hi-Chemical, Kanagawa, Japan), Aluminum foil (0070, Toyo Aluminum Ekco Products, Osaka, Japan) and LM under the conditions as indicated.

LM micro/nano particles were prepared by the following way. Briefly, LM (25 μL, ~100 mg) was mixed in distilled water (10 mL) by pulse-type sonication (VCX-600; Sonics, Danbury, CT, USA) for 10 min in ice bath with and without poly(ethylene glycol) methyl ether thiol (PEGMET) [number-average molecular weight M_n = 2,000; Aldrich, MO, USA) (10 mg)]. The product (LM concentration: ~20 mg mL^{-1}) was then used for further structural and exothermic characterizations. The structure of LM micro/nano particles with and without poly(ethylene glycol) methyl ether thiol was observed by a scanning electron microscopy (SEM) (VE-9800; Keyence, Osaka, Japan).

AMF−thermal conversion efficiency of LMs was determined according to the previous methods (Yonetsu et al., 2014; Ikemoto et al., 1986). Detailed calculation was given as following:

$$\eta = CVD(T2 - T1) / Pt \quad (1)$$

where η is the AMF−thermal conversion efficiency, C is the heat capacity of EGaIn (0.38 J g^{-1} °C^{-1}) (Majeski et al., 2010; Yu et al., 2014), V is the volume of EGaIn blob (3×10^{-8} m^3), D is the density of EGaIn (6.25×10^6 g m^{-3}) (Xu et al., 2012), and t is the heating time (60 sec). The attainment temperature (T2) of the distilled water of the LM blob after 60 sec was 35.1°C and initial temperature (T1) was 20.0°C. Herein, the temperature change (T2 – T1) of the water of the LM blob was 15.1°C.

The value of the power for heating (P) is defined as equation (2).

$$P \approx \frac{B^2 f^2}{R} \quad (2)$$

The magnetic flux density (B) can be calculated by equation (3). Meanwhile, f is the frequency of AMF (245×10^3 Hz). R is the electrical resistivity of water (18.3×10^4 Ω) (Kaye, G.W.C. et al., 1911).

$$B = \mu H \quad (3)$$

Where μ is the magnetic permeability of water (12.6×10^{-7} H m^{-1}) (Kaye, G.W.C. et al., 1911) and H is the magnetic field strength (200 A m^{-1}). The values of V, t, T_{atta}, T_{ini}, f, and H were obtained from Figure S4a.

Thus, substituting according values of each parameter to equation (1), AMF−thermal conversion efficiency (η) of the LM droplets can be calculated to be about 86.3%. The efficiencies at different times were also calculated by

the same way and summarized in Figure S4b.

Cell culture and viability assays

Human lung carcinoma (A549), colorectal adenocarcinoma (HT-29), bone osteosarcoma (U2OS), and normal diploid fibroblasts (TIG3) were obtained from JCRB Cell Bank or DS Pharma Biomedical (Tokyo, Japan) and cultured in Dulbecco's Modified Eagle's medium (DMEM) medium (Gibco BRL, Grand Island, NY, USA) with 10% fetal bovine serum, 2 mM L-glutamine, 1 mM sodium pyruvate, gentamycin, penicillin–streptomycin (100 IU mL^{-1}), and Hank's balanced salt solution (Life Technologies, MD, USA). Cells were maintained at 37°C in a humidified chamber at 5% CO_2.

Cell viability assays were conducted by crystal violet staining (Wako, Osaka, Japan) and using Cell Counting Kit-8 (CCK-8; Dojindo Laboratories, Kumamoto, Japan). For the crystal violet assays, cells were seeded in 6-well (2.5×10^5 cells $well^{-1}$) or 12-well (1.5×10^5 cells $well^{-1}$) plates the night before the treatment. After cell attachment, a LM droplet (25 µL) or the LM-Gel microdevice was added to the wells, followed by AMF exposure for the indicated period. The staining was carried out either immediately after the treatment or 24 h later. Prior to staining, the LM was removed and the cells were washed with cold PBS and fixed with a pre-chilled methanol/acetone (1:1) mixture for 10 min. The fixed cells were then incubated with 0.1% crystal violet solution overnight. For CCK-8 assays, cells were seeded in 24-well (5×10^4 cells $well^{-1}$) or 48-well (2×10^4 cells $well^{-1}$) plates. After 24 h, a 20-µL droplet of the LM was added for the as-indicated AMF treatment. After the LM was removed, the cells were washed with fresh medium and then incubated with CCK-8 solution according to the manufacturer's instructions. Absorbance at 450 nm was read on a microplate reader (Infinite M200 PRO, Tecan, Männedorf, Switzerland). All assays were performed independently at least three times.

***In vivo* magnetic hyperthermia therapy**

All animal experiments were performed strictly in accordance with protocols approved by the Institutional Animal Care and Use Committee of AIST. The HT-29 tumor-bearing C57BL/6NCrSlc mice (n = 5, female, 5 weeks old; Japan SLC, Shizuoka, Japan) were intratumorally injected with 30 µL of the LM when the tumor volumes reached approximately 250 mm^3. An equal volume of PBS buffer solution was applied as a control. Subsequently, the mice were exposed to an AMF (150 A m^{-1}, 245 kHz) for 5 min. During the AMF treatment, the temperature at the tumor site was measured by IR thermography. Tumor formation and mice health (body weight) was monitored every other day. The volume of the subcutaneous tumors was calculated as $V = L \times W^2/2$, where L and W are the length and width of the tumor, respectively.

***In vivo* viability evaluation**

Five-week-old female mice (n = 5; average weight = 18 g; C57BL/6NCrSlc) were provided by Japan SLC, Inc. (Shizuoka, Japan) and housed in a specific pathogen-free environment. Two hundred microliters of LM suspension (10 mg mL^{-1}, sonicated in PBS for 10 min) was administered to the mice by either oral feeding or intraperitoneal injection. The body weights of the mice were recorded every other day for 24 days.

Further LM biocompatibility tests were investigated as follows. LM or PBS was injected into the tail vein and

the back under the skin of a 10-week-old female mouse (n = 5; average weight = 21 g; BALB/cSlc; Japan SLC, Inc.). Volumes of injected LMs for subcutaneous administrations was 30 μL. Viability observations and weight determinations of injected mice were performed every twice a week for 60 days. Blood samples were collected from the inferior vena cava of the mouse after 28 days. CBC and biochemical examination were performed by Japan SLC, Inc. and Oriental Yeast Co., Ltd. (Tokyo, Japan).

The distribution behavior of injected LMs in living mice was analysed by Shin Nippon Biomedical Laboratories, Ltd. (Kagoshima, Japan) using the X-ray CT instrument (Asteion/S4; Toshiba Medical Systems, Tochigi, Japan). LM (30 μL) was subcutaneously injected into the back of 11-week-old male nude mice (n = 4; average weight = 21 g; BALB/cAJc-nu/nu, Japan SLC, Inc.). X-ray CT scanning was performed under anaesthesia of mice just after injection or after incubation for 7 days with injection. For biological distribution of LM via oral administration, five microliters of LM was administered to the 11-week-old male mice (n = 3; average weight = 22 g; BALB/cAJlc-nu/nu, Japan SLC, Inc.) by oral feeding. X-ray CT imaging of the mice, feces, and organs were performed for 24 h.

Simulation of AMF-induced subcutaneous LM transformation

A sandwich system consisted of glass slide – pig skin tissue – glass slide (from bottom to top) was assembled as shown in Figure S5. Briefly, 30 μL of LM was deposited on the inner face of pig skin (ca. 4 cm × 2.5 cm, Funakoshi, Tokyo, Japan) attaching on the bottom slide. The corners of the skin were subsequently coated with instant adhesive, so that the following top slide can be tightly covered on the skin. After 10 min for adhesive stabilization, the packed sandwich system was subjected to AMF exposure (100 A m^{-1}, 245 kHz) to observe the LM transformation.

Controlled release of RhB

The RhB (Wako)-loaded LM/hydrogel system was subjected to an aqueous environment to investigate AMF-induced RhB release. The aqueous solution volumes and AMF conditions were adjustable depending on the purposes of the experiment. In the case of RhB release in a glass vial, 2 mL of Milli-Q water was added to the LM/hydrogel depot (LM 20 μL; agarose 2% w w^{-1}; RhB 0.5 mg mL^{-1}) with a solidified volume of 1 mL; the vial was then placed on the coil for AMF exposure (200 A m^{-1}, 245 kHz). The AMF exposure time was set to 30 s for ON and 30 s for OFF, and the exposure was repeated for five cycles. At each interval, the temperature of the LM/hydrogel and the surrounding water was measured using a temperature sensor, whereas 10 μL of supernatant was collected for calculation of the release rate. The RhB release rate in the presence or absence of the AMF was measured on the basis of the concentration of released RhB calculated from the UV–Vis calibration curve in Figure S3a. The same RhB-loaded hydrogel depot without LM (replaced with PBS) was used as a negative control. For the long-termed RhB release experiment, the system was kept at 37°C for 3 days except when AMF was applied (1 min once per day).

Fabrication of the LM/hydrogel system

The volumes of agarose (Wako), LM, and RhB were adjusted depending on the type of container (glass vial or PCR tube). For instance, a LM/RhB-Gel microdevice was fabricated by dissolving 0.5 g of agarose in 25 mL of RhB aqueous solution (0.5 mg mL^{-1}) at 60°C, followed by vortex mixing. Then, 200 μL of molten agarose mixture was transferred into a PCR tube (ca. 2000 μm in length and 500 μm in width, Eppendorf, Hamburg, Germany) together

with 20 μL of the LM. The PCR tube was chilled at room temperature until the LM-loaded hydrogel depot solidified. The resultant fabricated drug delivery microdevice was enclosed with the PCR tube cap and stored at 4°C prior to further experiments.

References

Ikemoto, Y., Takahashi, A., and Hama, H. (1986). Temperature distribution of flying pan heated with a magnetic induction heating cooker and it thermal efficiency. Kaseigakuzashi *37*, 949–954.

Kaye, G.W.C., and Laby, T.H. (1911) Table of physical and chemical constants and some mathematical functions. National Physical Laboratory.

Majeski, R. (2010). Liquid metal walls, lithium, and low recycling boundary conditions in tokamaks. AIP Conf. Proc. *1237*, 122.

Yonetsu, D., and Yamamoto, Y. J. (2014). Caluculation of heating efficiency of induction heating cooker by using finite element analysis. IEIE Jpn. *34*, 339–345.

Yu, S., and Kaviany, M., (2014). Electrical, thermal, and species transport properties of liquid eutectic Ga-In and Ga-In-Sn from first principles. J. Chem. Phys. *140*, 064303.

Xu, Q., Oudalov, N., Guo, Q., Jaeger, H.M., and Brown, E. (2012). Effect of oxidation on the mechanical properties of liquid gallium and eutectic gallium-indium. Phys. Fluids *24*, 063101.